Heliyon 9 (2023) e13850

Contents lists available at ScienceDirect

Heliyon

journal homepage: www.cell.com/heliyon

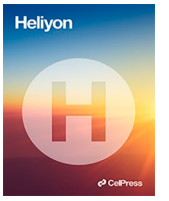

Research article

Influence of thermal conductivity on transient mixed convection in a vented cavity with a hollow cylinder and filled with CNT-water nanofluid

Mohedul Hasan [a,b], Shadman Sakib Priam [c], Abrar Nur-E Faiaz [c], A.K. Azad [d], M.M. Rahman [a,*]

[a] Department of Mathematics, Bangladesh University of Engineering and Technology, Dhaka 1000, Bangladesh
[b] Department of Mathematics, Dhaka University of Engineering and Technology, Gazipur, Bangladesh
[c] Department of Mechanical Engineering, Bangladesh University of Engineering and Technology, Dhaka 1000, Bangladesh
[d] Department of Natural Sciences, Islamic Universality of Technology, Gazipur, 1704, Bangladesh

ARTICLE INFO

Keywords:
Thermal conductivity
Transient mixed convection
CNT water Nanofluid
Finite element method
Vented cavity

ABSTRACT

This study is aimed to perform a numerical time-dependent investigation thermal conductivity effect of the annular cylinder within a vented cavity using CNT based-water nanofluid. For demonstrating the effect of thermal conductivity, four distinct hollow cylinder materials such as Ks = 0.5(Plastic tiles), Ks = 0.84(Clay tiles), Ks = 1.1(Concrete tiles), and Ks = 2(Slate tiles) are introduced together with a suitable variation of dimensionless time ($0 \leq \tau \leq 1$). The governing equations of the model with associated boundary conditions is solved using finite element based Galerkin's weighted residual method. Different contour plots for thermal and flow field transformation and mean Nusselt number, mean fluid temperature, bulk convective field temperature, temperature gradient, pressure gradient, vortices, and fluid velocity magnitude are presented for qualitative and quantitative thermal performance analysis. With the decrease of solid thermal conductivity, 27.3% thermal transport enhancement is noted from the heated surface of the cylinder. However, a 16.3% increase in the bulk fluid temperature has been recorded with the increase in cylinder conductivity. The numerical outcomes from this investigation propose a better thermo-fluid efficiency compared to the existing methodology which can be suggestive to engineers and researchers for designing heat exchangers, heat pipes, and other thermal systems.

1. Introduction

Conjugate heat transfer in a square cavity has been given a lot of focus in recent years to make the environment smooth leaving within the COVID-19 pandemic situation. Also, this focus is because of the large range of significant applications involving natural resources of processes of convection. These applications cover a broad range of topics such as solar-based energy harvesting, safety, and operation of nuclear reactors, designing energy-efficient parts such as buildings, rooms, and machinery, and the prevention and safety of fires [1–3] The placement and dimensions of the doors and windows, for example, engage in a crucial role in the distribution and expansion of products of combustion in a chamber. The existence of ports in the casing also significantly improves the cooling of

* Corresponding author.
E-mail addresses: m71ramath@gmail.com, mmustafizurrahman@math.buet.ac.bd (M.M. Rahman).

https://doi.org/10.1016/j.heliyon.2023.e13850
Received 13 May 2022; Received in revised form 9 February 2023; Accepted 13 February 2023
Available online 18 February 2023

Nomenclature

A	non dimensional fluid area
c_p	specific heat capacitance (J/kgK)
D_i	inner diameter of cylinder (m)
d	average diameter of cylinder (m)
g	gravitational acceleration (m/s^2)
k	thermal conductivity (W/mK)
Ks	thermal conductivity of solid (W/mK)
L	length of the cavity (m)
N	non-dimensional wall-normal length
Nu	Nusselt number
p	dimensional fluid pressure (Pa)
P	non-dimensional fluid pressure
Pr	Prandtl number
Ra	Rayleigh number
Re	Reynolds number
Ri	Richardson number
Sr	non-dimensional shear rate
T	dimensional temperature (K)
t	dimensional time (s)
x,y	Cartesian coordinates (m)
X,Y	non-dimensional Cartesian coordinates
u,v	dimensional velocity components (m/s)
U,V	non-dimensional velocity components
D_o	outer diameter of cylinder (m)

Greek symbols

&ohm	vorticity magnitude
∇P	non-dimensional pressure gradient
$\nabla\theta$	non-dimensional temperature gradient
α	thermal diffusivity (m^2/s)
β	thermal expansion coefficient (1/k)
μ	fluid dynamic viscosity (kg/ms)
τ	non-dimensional time
φ	nanoparticle volume fraction
ρ	fluid density (kg/m^3)
θ	non-dimensional temperature

Subscripts

av	average
exit	exit port
c	cold
f	base fluid
i	inlet port
h	hot
s	solid
nf	nanofluid

electrical parts.

It is worth noting that the cavity walls imposed with different types of thermal conditions can have a massive impact on natural convection. Not only numerical but also analytical studies are carried out by November and Nansteel [4] to investigate buoyancy-induced convection happening inside a square cavity filled with water. In their investigation, higher temperature was applied on the bottom wall and lower temperature on a vertical wall of the cavity. Valencia and Frederick [5] numerically studied free convective flow of air-filled square enclosure for varying Rayleigh According to their studies, peak heat transfer performance was found at Rayleigh's number around 10^5 because of the substantial conduction effect. House et al. [6] experimented with the help of a centrally positioned thermally conductive body in a square vertical cavity to demonstrate the influence of a heat-conducting body in the cavity. They observed that only when the body which is doing the work of conduction had a thermal conductivity ratio of less than 1, the development of heat exchange everywhere in the cavity becomes profound. Hussein et al. [7] studied mixed convection laminar flow in a trapezoidal cavity using nanofluid with porous media and rotating inner circular cylinder. In their investigation, Nu_{av}

increased with increasing *Ra* and *D*, inner cylinder radius, solid volume fraction, and angular rotational velocity of the cylinder, but decreased with increasing porous layer thickness and the number of undulations. Laouria et al. [8] investigated the heat transfer characteristics for a trapezoidal cavity with horizontal channel and heat source. The results revealed that the length of the heat source had a significant influence on the distribution of isotherms. It was also discovered that as the length of the local heat source increased, so did the local and average Nusselt values. The highest temperature was also found near the heat source. In a study headed by Al-Rashed et al. [9] a cavity was heated by a centrally positioned isothermal block, and the outcomes of convective energy transfer and entropy generation were shown using particle trajectories, isotherms, Nusselt number, and Bejan number. For all Richardson numbers, increasing the concentration of nanoparticles enhanced thermal entropy creation, while the variance in viscous irreversibility with concentrations was dependent on Ri variation. Ahmed et al. [10] investigated a continuous laminar two-dimensional MHD mixed convection in a square-angled cavity filled with Cu-water nanofluid using the finite difference method. When the magnetic field had such a small influence, the nanofluid outperformed water in terms of heat transport, whereas when the magnetic field had a large influence, water outperformed the nanofluid. According to the findings, the partial slide had a significant influence on the aforementioned indicators. Basak et al. [11] examined the effect of a square cavity's bottom wall that was uniformly and non-uniformly heated at the same time. The cavity's vertical walls were cold, and the top wall was in an adiabatic state, maintaining a constant temperature. They noticed that the heat transfer rate was significantly lower for non-uniform cases by varying both the *Ra* and the *Pr*. Following extensive research on natural convection, the majority of works moved on to forced convection. According to the review study [12], mixed convection with different fluids was shown to be more efficient heat transfer fluids than single nanoparticle-based nanofluids or conventional fluids. Izadi et al. [12] divided the publications in this review into four categories: square (and rectangular), triangular, trapezoidal, and unusual forms, and then summarized their key findings in a table. The majority of investigations revealed that incorporating nanoparticles into the base fluids improved heat transfer by increasing the nanoparticle volume concentration, Richardson number, and Reynolds number, as well as the necessary pumping power.

Because of their widespread application in industry, nanofluids in a vented square cavity with differentially heated and sinusoidal solid partitions play an important role. Al-Kouz et al. [13] investigated entropy generation and mixed convective heat transfer in a three-dimensional cavity containing a revolving cylinder filled with a phase change material (PCM). The temperature difference between the hot right vertical wall and the cool left vertical wall was produced, while the remaining walls were regarded as adiabatic. The insertion of an external magnetic field resulted in a decrease in heat exchanges because of produced Lorentz force, which reduces Buoyancy effect. Priam and Nasrin [14] studied the entropy generation and magneto-hydrodynamic conjugate convective heat transfer of a hybrid nanofluid (Ag–MgO-water) and noticed that the magnetic effect and cavity position angle have a significant impact on thermal behavior and entropy generation. Furthermore, the effects of the corrugated partition's solid thermal conductivity on thermal performance control were observed in the research of Priam et al. [15] in an air-water partitioned enclosure. Sundar et al. [16] presented a review on the synthesizing of hybrid nanoparticles, the formation of hybrid nanofluids, thermal characteristics, heat transfer, friction factor, and the current Nusselt number and friction factor correlations. Saeidi and Khodadadi [17] investigated shallow enclosures with varying inlet dimensions and outlet placements to account for forced convection. They discovered that parallel placement of the inlet and outlet caused less pressure drop and that placing the outlet port at the end of three corners produced the highest Nusselt number. Using a finite element model, Ali et al. [18] looked into the influence of Dufour and Soret on the magneto-hydrodynamic rotational flow using Oldroyd-B nanofluid on a stretched sheet for double diffusion. They increased the parameters for magnetic force, Deborah number, and rotating fluid, which slowed the main and secondary velocities but increased the temperature in the same way that thermophoresis and Brownian motion do. Selimefendigil and Öztop [19] investigated forced convection in a ferrofluid-filled two-dimensional ventilated square cavity with an adiabatic rotating cylinder numerically. According to the findings, the length and dimensions of the flow regime can be restrained by the magnetic dipole intensity and circular rotating rate of the cylinder by varying the width-to-height aspect ratio and the Rayleigh number. Iwatsu et al. [20] pioneered mixed convection by investigating the flow and heat transfer of a viscous fluid inside a cavity with a stable vertical temperature gradient. Singh and Sharif [21] expanded on their previous work by considering not only six possible placement settings of the intake and exit terminals of a differentially heated enclosure but also mixed convection, whereas the previous study only considered two distinct inlet and exit port combinations. The heat transfer features of a circular cylinder positioned in a vertical lid-driven chamber for mixed convective transport have been significantly influenced by the cylinder's rotating speed. In their investigation, Chatterjee et al. [22] observed this tendency. The results showed that rotational speed had no effect on the drag coefficient. The average Nusselt number for the heated wall increased when rotated counterclockwise, while it decreased when rotated clockwise.

The heat exchange rate was increased with increasing rotational velocity in both cases of clockwise and anti-clockwise directions when the MHD (Magento Hydro Dynamic) impact was considerable. The magneto-hydrodynamic flow of a Ag_2Al based water nanofluid in a corrugated trapezoidal enclosure containing a heat-generating rotating solid cylinder was studied by Job et al. [23]. The flow circulation zones surrounding the revolving cylinder were improved with increasing nanoparticle sizes and cylinder radius, according to the findings of this study. Consequently, with smaller nanoparticle sizes and a larger cylinder radius, the nanofluid temperature and energy transport increased. Rahman et al. [24] conducted numerical research for mixed convection in a cavity which was rectangular in the physical dimension and held a thermally conductive circular-sized cylinder. It was noted that the dimension of both the opening and the circular cylinder along with the thermal conductivity ratio of the cylinder played a vital contribution while showing the results of the heat transfer rate Using a computational model, Lacroix and Joyeux [25] investigated heat transfer for natural convective characteristics from two vertically positioned and separately heated cylinders in a rectangular cavity. This cavity received cooling from above. Lacroix and Joyeux [26] also performed a computational analysis of natural convection heat transport from two cylinders that were not only horizontally positioned but also heated and enclosed within a rectangular cavity with finite wall conductance. According to the researchers, wall heat conduction reduces average temperature fluctuations throughout the hollow,

slows the flow, and reduces natural convection heat transfer in all directions of the cylinders. Butler et al. [27] investigated the effect of a heat-generating cylinder placed inside a square enclosure with a differentially heated vertical wall. Heat transfer from the cylinder deviated from the correlations available in previous works of literature as the Rayleigh number increased. Estellé et al. [28] predicted the average Nusselt number of a square cavity that was differentially heated and topped up with both Newtonian and non-Newtonian CNT nanofluids. Increased nanoparticle content, which has been linked to both non-Newtonian properties of nanofluids and temperature rise, has been shown to reduce the Nusselt number of nanofluids. Al-Rashed et al. [29] studied the impact of an external magnetic force's angle of inclination on free convection within a cube shape cavity charged with CNT-based water nanofluid using volume as a base for a three-dimensional numerical model. Heat transmission is shown to increase in intensity as the fraction of CNT particles increases and the Rayleigh number increases. Hamid et al. [30] investigated natural convection within the confines of a partially warmed-up rectangular enclosure that is fin-shaped and contains a cylindrical obstacle. Water-based CNT was used to fill the cavity. It is demonstrated that by including not only a solid volume fraction of CNTs but also radiation effects, the local Nusselt numbers are increased, with the highest Nusselt number at the corners. Selimefendigil and Öztop [31] numerically investigated free convection within an enclosure with a grooved partition using different fluids. In one of the domains, an inclined uniform magnetic field was applied to a carbon nanotube (CNT)-water nanofluid. The Nusselt number improved significantly when CNTs were used. As the Hartmann number increased, the average heat transfer decreased, but it fluctuated slightly as the magnetic inclination angle changed. Gupta et al. [32] discovered that the presence of a circular cylinder with prominent conduction properties, cylinder size, thermal conductivity ratio, and temperature conditions of the enclosure walls all had a significant influence on the situation of mixed convection. Priam et al. [33] demonstrated that a CCW (counterclockwise) spin of an isothermally heated spinning cylinder inside a square vented enclosure provided a higher heat transfer rate than any other location of the cylinder. Faiaz et al. [34] investigated mixed convection for Gallium flow in a square cavity that was partially vented with the presence of a rotating cylinder in the centre. When the Richardson number increased, the heat transfer rate decreased while the average bulk fluid temperature increased. Mamun et al. [35] ran a numerical for mixed convection for a hot hollow cylinder in a cavity with an inlet and an outlet. The cylinder diameter appears to have a significant impact on both the flow and thermal fields, whereas the solid-fluid thermal conductivity ratio appears to have a significant impact on the thermal field only. Tayebi and Chamkha [36] investigated entropy production and natural convection flow in a square enclosure with a magnetic field and a conductive hollow cylinder in the cavity using Cu–Al_2O_3/water hybrid nanofluid as the fluid domain. Later, extensive studies [37,38] on mixed convection were conducted by researchers with varying thermo-physical properties, governing parameters, and geometric shapes to capture the effects of those variations on heat transfer evaluation. Ismael et al. [39] investigated the role of fluid-structure interaction (FSI) in mixed convection in a square chamber with two inlet and exit apertures. The researchers discovered that a flexible fin improved the Nusselt number more than a rigid fin. The shape of the fin and the Nusselt number reached a steady periodic state at higher levels of the Cauchy and Richardson numbers.

According to the aforementioned review, much research has been done on mixed convection in a cavity with a hollow cylinder. The effects of different nanofluids, cylinder diameter size, and boundary condition variation were also discussed. To the best of the author's knowledge, however, a hollow cylinder made of various tile materials and placed inside a square cavity has yet to be discovered. As a result, the authors of this study assessed the impact of four different tile materials used to form a hollow cylinder that was then placed inside a square cavity filled with water-CNT nanofluid. The thermophysical and hydrodynamic properties of the considered model were also investigated. Nuclear reactor fuel rods, oil well drilling, and rotating tube heat exchangers can all benefit from the effect of thermal conductivity on transient mixed convection in a vented cavity filled with CNT-Water nanofluid. The results of this study can be used to determine the best flow and parameter combinations for improving heat transfer in those system applications.

2. Methodology

2.1. Model description

A 2D square cavity with length "L" is taken for this research. The bottom wall of the cavity is considered *x*-axis while the left vertical wall is assumed to y-axis. In the center of the cavity is a heated annular hollow cylinder. The inner and the outer diameter of the cylinder are 0.1L and 0.3L respectively. The inner surface of the cylinder is at a constant high temperature T_h. As the cylinder material is assumed to be heat-conducting in nature, the outer surface is considered a continuous conductive surface by the inner surface. An inlet port of dimension $W = 0.2L$ is considered at the upper side of the left vertical wall whereas the upper side of the right vertical wall indicates the cavity's outlet with the same dimension. Water-based CNT nanofluid is entering inside the cavity with constant temperature T_c as a working fluid and the thermophysical property of the nanofluid is presented in Table 1 taken from Ref. [40]. Volume fraction of the nanofluid used is $\varphi = 2\%$. All the other walls of the cavity are adiabatic in nature and the no-slip condition is held accountable for this scenario. Water-based CNT single phase nanofluid is thought to be Newtonian, incompressible, laminar flow and unsteady in nature. The Boussinesq approximation is used for this study. The fluid's Joule heating effect and viscous dissipation effect are however negligible. The y-axis is adjusted to a negative value for gravity's acceleration (g). The model's setup and boundary

Table 1
Thermophysical properties of the fluid and solid phase [40].

Properties	c_p (J/kg K)	p (kg/m^3)	k (W/m K)	β (K^{-1})
Fluid (water)	*4179*	9 97.1	0.613	2.1×10^{-4}
Solid (CNT)	650	1350	3500	4.2×10^{-5}

conditions are shown in Fig. 1.

2.2. Governing equations and boundary conditions

The two-dimensional equations for continuity, momentum for x and y-axis, and energy for fluid domain are as follows:

$$\frac{\partial u}{\partial x}+\frac{\partial v}{\partial y}=0 \tag{1}$$

$$\rho_{nf}\left(\frac{\partial u}{\partial t}+u\frac{\partial u}{\partial x}+v\frac{\partial u}{\partial y}\right)=-\frac{\partial p}{\partial x}+\mu_{nf}\left(\frac{\partial^2 u}{\partial x^2}+\frac{\partial^2 u}{\partial y^2}\right) \tag{2}$$

$$\rho_{nf}\left(\frac{\partial v}{\partial t}+u\frac{\partial v}{\partial x}+v\frac{\partial v}{\partial y}\right)=-\frac{\partial p}{\partial y}+\mu_{nf}\left(\frac{\partial^2 v}{\partial x^2}+\frac{\partial^2 v}{\partial y^2}\right)+(\rho\beta)_{nf}g(T-T_i) \tag{3}$$

$$\frac{\partial T}{\partial t}+u\frac{\partial T}{\partial x}+v\frac{\partial T}{\partial y}=\alpha_{nf}\left(\frac{\partial^2 T}{\partial x^2}+\frac{\partial^2 T}{\partial y^2}\right) \tag{4}$$

For the solid domain, the energy equation is:

$$\frac{\partial T_s}{\partial t}=\alpha_s\left(\frac{\partial^2 T_s}{\partial x^2}+\frac{\partial^2 T_s}{\partial y^2}\right) \tag{5}$$

Boundary conditions with dimensions are given in Equation. (6):

$$\left.\begin{array}{l}\text{At } t=0: u=v=0, T=0, p=o\\ \text{At } t>0: \text{On cavity}: u=v=0, \dfrac{\partial T}{\partial N}=0 \text{ when } 0\le x\le L; y=0, L\\ u=0=v, \dfrac{\partial T}{\partial N}=0 \quad \text{when } x=0, L;\ 0\le y\le \dfrac{4}{5}L\\ u=u_i, v=0, T=T_c \text{ when } x=0;\ \dfrac{4}{5}L\le y\le L\\ \qquad\qquad \text{outlet : convective boundary}\\ \text{condition}, p=0 \text{ when } x=L;\ \dfrac{4}{5}L\le y\le L\\ \text{On cylinder : fluid}-\text{solid interface}, u=v=0, k_{nf}\left(\dfrac{\partial T}{\partial N}\right)_{nf}=k_s\left(\dfrac{\partial T}{\partial N}\right)_s\\ \text{inner surfaceu}, \mathrm{u}=v=0, T=T_h\end{array}\right\} \tag{6}$$

Equations (1) to (5) are scaled using the following variables in Equation (7):

$$(X,Y)=\frac{(x,y)}{L}, (U,V)=\frac{(u,v)}{u_i}, P=\frac{p}{\rho u_i^2}, \theta=\frac{T-T_i}{T_h-T_i}, \tau=\frac{u_i t}{L} \tag{7}$$

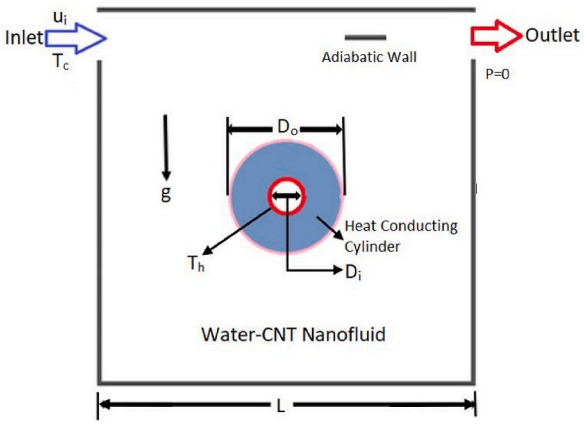

Fig. 1. Schematic model of the considered problem.

Here, associated symbols and variables have described in nomenclature.

For the derivation of non-dimensional equations (9) to (13) for equations (1) to (5), several controlling parameters are used. Reynolds number (Re), Prandtl number (Pr), Rayleigh number (Ra), and Richardson number (Ri) are four such parameters are given in Equation (8). The parameters that are defined are as follows:

$$Re = \frac{u_i L}{\nu_f}, Pr = \left(\frac{\nu}{\alpha}\right)_f, Ra = \frac{g\beta_f (T_h - T_i) L^3}{(\nu\alpha)_f}, Ri = \frac{Ra}{PrRe^2} \tag{8}$$

The non-dimensional versions of the governing equations stated in equations (1) to (5) that have been developed after applying these parameters are:

$$\frac{\partial U}{\partial X} + \frac{\partial V}{\partial Y} = 0 \tag{9}$$

$$\frac{\rho_{nf}}{\rho_f}\left(\frac{\partial U}{\partial \tau} + U\frac{\partial U}{\partial X} + V\frac{\partial U}{\partial Y}\right) = -\frac{\partial P}{\partial X} + \frac{\mu_{nf}}{\mu_f}\frac{1}{Re}\left(\frac{\partial^2 U}{\partial X^2} + \frac{\partial^2 U}{\partial Y^2}\right) \tag{10}$$

$$\frac{\rho_{nf}}{\rho_f}\left(\frac{\partial V}{\partial \tau} + U\frac{\partial V}{\partial X} + V\frac{\partial V}{\partial Y}\right) = -\frac{\partial P}{\partial Y} + \frac{\mu_{nf}}{\mu_f}\frac{1}{Re}\left(\frac{\partial^2 V}{\partial X^2} + \frac{\partial^2 V}{\partial Y^2}\right) + \frac{(\rho\beta)_{nf}}{(\rho\beta)_f} Ri\theta \tag{11}$$

$$\frac{\partial \theta}{\partial \tau} + U\frac{\partial \theta}{\partial X} + V\frac{\partial \theta}{\partial Y} = \frac{\alpha_{nf}}{\alpha_f}\frac{1}{RePr}\left(\frac{\partial^2 \theta}{\partial X^2} + \frac{\partial^2 \theta}{\partial Y^2}\right) \tag{12}$$

$$\frac{\partial \theta_s}{\partial \tau} = \frac{\alpha_s}{\alpha_f}\frac{1}{RePr}\left(\frac{\partial^2 \theta_s}{\partial X^2} + \frac{\partial^2 \theta_s}{\partial Y^2}\right) \tag{13}$$

The following Equation (14) is the study's non-dimensional boundary conditions:

$$\left.\begin{array}{l} \text{At } \tau = 0 : U = V = 0;\ \theta = 0;\ P = 0 \\ \text{At } \tau > 0 : \text{On cavity} : U = V = 0;\ \dfrac{\partial \theta}{\partial N} = 0 \text{ when } 0 \le X \le 1; Y = 0, 1 \\ U = V = 0, \dfrac{\partial \theta}{\partial N} = 0 \quad \text{when } X = 0, 1;\ 0 \le y \le 0.8 \\ U = 1, V = 0, \theta = 0 \text{ when } X = 0;\ 0.8 \le Y \le 1 \\ \qquad\qquad \text{outlet : convective boundary} \\ \text{condition}, P = 0 \text{ when } X = 1;\ 0.8 \le Y \le 1 \\ \text{On cylinder : fluid} - \text{solid interface}, U = V = 0, k_{nf}\left(\dfrac{\partial \theta}{\partial N}\right)_{nf} = k_s\left(\dfrac{\partial \theta}{\partial N}\right)_s \\ \text{inner surfaceu}, \mathrm{U} = V = 0, \theta = 1 \end{array}\right\} \tag{14}$$

2.3. Nanofluid models

Different formulae for calculating the values of nanofluid parameters such as viscosity μ_{nf}, effective density ρ_{nf}, specific heat $(c_p)_{nf}$, thermal diffusivity α_{nf}, and thermal expansion coefficient β_{nf} are also stated in the following Equations (15) – (18), also reported in Rumman et al. [41] as below:

$$\rho_{nf} = (1 - \varphi)\rho_f + \varphi\rho_s \tag{15}$$

$$(\rho c_p)_{nf} = (1 - \varphi)(\rho c_p)_f + \varphi(\rho c_p)_s \tag{16}$$

$$\alpha_{nf} = \frac{k_{nf}}{(\rho c_p)_{nf}} \tag{17}$$

$$(\rho\beta)_{nf} = (1 - \varphi)(\rho\beta)_f + \varphi(\rho\beta)_s \tag{18}$$

The Maxwell (thermal static conductivity) model ignores Brownian motion particles. However, the Brownian motion of particles is shown a clear advantage over the thermal transport capacity of nanofluids in experiments. Kalbani et al. [42] proposed a model for determining nanofluid thermal conductivity that takes into account both static and Brownian motion is given in Equations (19)–(21).

$$k_{nf} = k_{static} + k_{Brownian} \tag{19}$$

$$k_{Brownian} = \frac{\varphi \rho_p c_{p,p}}{2} \sqrt{\frac{2K_B T_{ref}}{3\pi d \mu_{static}}} \tag{20}$$

$$k_{nf} = \frac{k_s + 2k_f - 2\varphi(k_f - k_s)}{k_s + 2k\varphi(k_f - k_s)} k_f + \frac{\varphi \rho_p c_{p,p}}{2} \sqrt{\frac{2K_B T_{ref}}{3\pi d \mu_{static}}} \tag{21}$$

The authors applied effective viscosity in their investigation, rather than using the Brinkman model based on Rumman et al. [43], also mentioned in Equation (22):

$$\mu_{nf} = \mu_{static} + \mu_{Brownian} = \frac{\mu_f}{(1-\varphi)^{2.5}} + \frac{k_{Brownian}}{k_f} \times \frac{\mu_f}{\mathrm{Pr}_f} \tag{22}$$

2.4. Formula to calculate hydrodynamic and physical properties

The equations for calculating hydrodynamic and physical properties considered in this study are given below in Equations (23) – (31):

Average Nusselt Number of Heated Cylinder Surface:

$$Nu_{av} = -\frac{L}{\pi d} \times \frac{k_{nf}}{k_f} \int_0^{\frac{\pi d}{L}} \left(\frac{\partial \theta}{\partial N} \right) dS \tag{23}$$

Shear Rate:

$$Sr = \frac{L}{\pi d} \int_0^{\frac{\pi d}{L}} \sqrt{\left(\frac{\partial U}{\partial X}\right)^2 + \left(\frac{\partial V}{\partial X}\right)^2} dS \tag{24}$$

Temperature Gradient:
Fluid domain:

$$\nabla \theta_f = \iint_{A_f} \sqrt{{\theta_{x,f}}^2 + {\theta_{y,f}}^2} dA \tag{25}$$

Solid domain:

$$\nabla \theta_s = \iint_{A_s} \sqrt{{\theta_{x,s}}^2 + {\theta_{y,s}}^2} dA \tag{26}$$

Pressure Gradient in Fluid Domain:

$$\nabla P = \iint_{A} \sqrt{{P_x}^2 + {P_y}^2} dA \tag{27}$$

Root Mean Square (RMS) Velocity in Fluid Domain:

$$RMS\ Velocity = \sqrt{U^2 + V^2} \tag{28}$$

Exit Port Fluid Temperature:

$$\theta_{exit} = \iint_{A_{exit}} \frac{\theta}{A_{exit}} dA \tag{29}$$

Vorticity Magnitude:

$$\Omega = \frac{\partial V}{\partial X} - \frac{\partial U}{\partial Y} \tag{30}$$

Bulk Temperature of Fluid Domain [44]:

$$\theta_b = \frac{\iint_A \frac{\theta}{\rho_{nf}} dA}{\iint_A \frac{1}{\rho_{nf}} dA} \tag{31}$$

3. Numerical operation

For obtaining the set of linear equations, the Galerkin finite element method based is incorporated for solving the non-dimensional governing equations 9–13 with the related boundary conditions (14). To describe the domain for Finite Element calculation, a triangular-based six-node element was used. To obtain the numerical solution, the Boussinesq Approximation was used for the iteration technique. The iteration method was repeated until the solution became convergent. The condition is subjected to the convergent condition $\left|\Phi^{n+1} - \Phi^{n}\right| \leq 10^{-6}$, n denotes the number of iterations and phi denotes general dependent variable. Detailed the finite element calculation is available in [45]

3.1. Grid sensitivity test

For ensuring numerical efficiency and optimizing computational runtime expenses, a grid sensitivity test is provided in the present analysis. A non-uniform triangle-based discretization technique has been applied for the subdivision of the computational domain. Three nodal points along with six degrees of freedom have been ensured where two degrees of freedom are covered by each node. For providing a better understanding of thermo-physical flow and thermal attributes at the higher gradient, refined grids are applied at solid-fluid and flow separating interactive boundaries. For determining the optimal grid, the changes of spatially averaged *Nu* and exit port temperature are taken as a sensitivity measure with the variation of element numbers for a reference case of Re = 100, Ri = 1, Pr = 6.7, Ks = 1, and τ = 0.2 which is shown in Fig. 2. Increasing trends from both Nusselt number and exit temperature were observed whereas the optimum element number has been found as 6285. Beyond this critical value of element number, hardly any change in thermal performance and thermo-fluid characteristics have been noted.

3.2. Code validation

For confirming the necessary substantiation of computational scheme, the present model is supposed to be verified with resembling previously published analyses. As the proof of numerical accuracy of the utilized computational approach, the ongoing model is backed with the outcomes from the numerical investigation of Chamkha et al. [46]. In this research, laminar mixed convection has been analyzed in an air-filled square vented with the insertion of a heated square cylinder. The thermal efficiency has been observed through the assessment of not only the average *Nu* but also average fluid temperature. Findings of this particular assessment, compared in terms of average Nusselt number along the heated surface and bulk average temperature, are shown in Fig. 3 against a variation of Ri at L_x = 0.5, L_y = 0.5, AR = 0.2, and Re = 200 for CT configuration. Moreover, the current simulation procedure has been validated against the investigation of Shirvan et al. [47] where optimization of mixed convection heat transfer has been prioritized in a Cu-water filled vented cavity by applying a variation of nanoparticle volume fraction, Richardson number, and inlet and outlet port locations. Table 2 presents a comparison of Mean *Nu* between the current numerical scheme and Shirvan et al. [47] fixing parameters at Ri = 0.1, H' = 0 and H" = 0.9H.

Both verifications are found to be in strong compliance with the prior works that have been published.

4. Results discussions

CNT water nanofluid with four different thermal conductivity of the solid (Ks = 0.5, 0.84, 1.1, and 2) as well as a variation of dimensionless τ from 0 to 1 is analyzed in a squared cavity containing a heated hollow cylinder. Values of thermal conductivities are taken based on material property of Ks = 0.5(Plastic tiles), Ks = 0.84(Clay tiles), Ks = 1.1(Concrete tiles) and Ks = 2(Slate tiles). In this section, the effects of thermal conductivity of solid (Ks) relating mixed convection have been analyzed from different thermo-physical

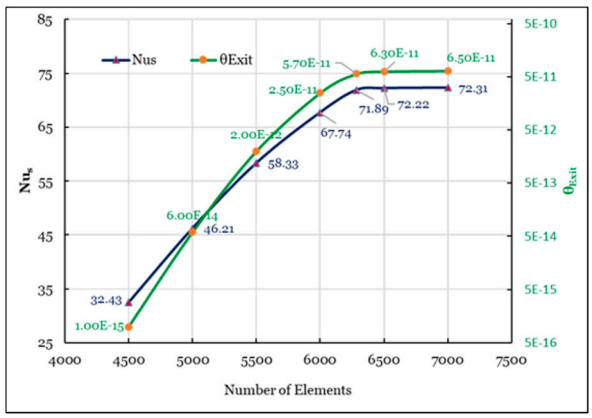

Fig. 2. Grid Test on average heat transfer of solid and average exit temperature at Re = 100, Ri = 1, Pr = 6.7, Ks = 1 and τ = 1.

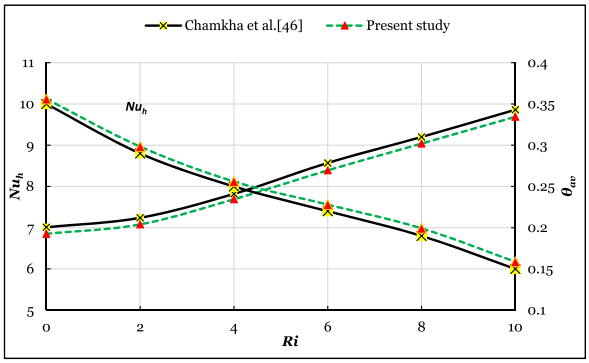

Fig. 3. Comparison of heated surface's Nusselt number and average temperature on Richardson number of the domain at Lx = 0.5, Ly = 0.5, AR = 0.2 and Re = 200 for CT configuration with Chamkha et al. [46].

Table 2
Comparison of Mean *Nu* on particle concentration for optimum convection at Ri = 0.1, H' = 0 and H" = 0.9H.

φ (%)	Shirvan et al. [47]	Present study	Error (%)
0	179.4319	175.3741	2.26%
1	161.2152	155.8064	3.36%
3	190.9468	186.2792	2.44%
5	146.5463	143.0541	2.38%

and hydrodynamic perspectives.

4.1. Effect on flow movement

Fig. 4 describes the outcome of thermal conductivity (Ks) of the hollow cylinder on the streamlines for three different cases of dimensionless time (τ). With the increase of Ks at τ = 0.1, insignificant changes throughout the streamlined plot except for the dimensions of the recirculation zone which is situated at the hollow cylinder's base. The recirculation zone is just starting to form here. But a notable increase in vorticity is seen for dimensionless time τ = 0.5, where increasing the Ks from 0.5 to 1.1 increases the effectiveness of the recirculation zone by 33%. As higher thermal conductivity enhances the better thermal efficiency and better heat transfer decreases the density of the working fluid. A similar trend has been observed for the particular incident of dimensionless time τ = 1. In addition, inner portion of the cavity, anti-clockwise vortex which is at the bottom of the hollow cylinder grows stronger with the passage of τ for a certain value of the thermal conductivity of the material. The rise in heat conductivity follows the same pattern. As the greater possibility of shifting vortex initially stored potential energy to the evolved kinetic energy. Despite the vortex being observed as an indicator of the fluid potential strength, the enhanced establishment of vortices in a particular zone paves a way for better flow energy transfer in the current research. From Fig. 4, the variation of solid thermal conductivity influences the fluid flow movement in such a way that a larger value of Ks provides a bigger degree of flow strength due to the density effect.

4.2. Effect on isotherm distortion

The influence of thermal conductivity (Ks) of four distinct materials and three different scenarios of dimensionless time on isotherms is illustrated in Fig. 5. The figure clearly shows how solid conductivity influences convective heat transport throughout the fluid domain. Fluid temperature changes along with the circular profile as the thermal conductivity of the material increases, similar to the vorticity of the fluid flow. As the inner surface of the hollow cylinder is heated, how much heat will reach the outside wall of the hollow cylinder and then pass through the fluid is supposed to be dependent on how much heat is conducted by the cylinder material. Due to a low value of Ks, a lot of isotherm lines can be seen inside the solid part of the cylinder while for the higher values of Ks, all the isotherm contours are on the profile of the outside of the hollow cylinder. As for the case of increment of dimensionless time τ, the isothermal contours are more distorted in a circular manner alongside the vicinity of the cylinder inside the cavity. The possible reason behind this is that as time passed, the heat outside the cylinder wall will likely be taken away by the water-based CNT fluid inside the cavity. From the thickening of isotherms, it can be conjectured that the thermal conductivity of solid has a significant influence on the isotherms because after raising the Ks from 0.5 to 2, the fluid temperature within the reach of the cylinder wall is nearly tripled.

4.3. Effect on the heat transfer rate

The significance of solid thermal conductivity (Ks), and dimensionless time (τ) on the average Nusselt number taken with respect to heated surface of the cylinder (Nu_{av}) can be noticed in Fig. 6. First observation to derive from Fig. 6 is that the value of Nu_{av} is decreased

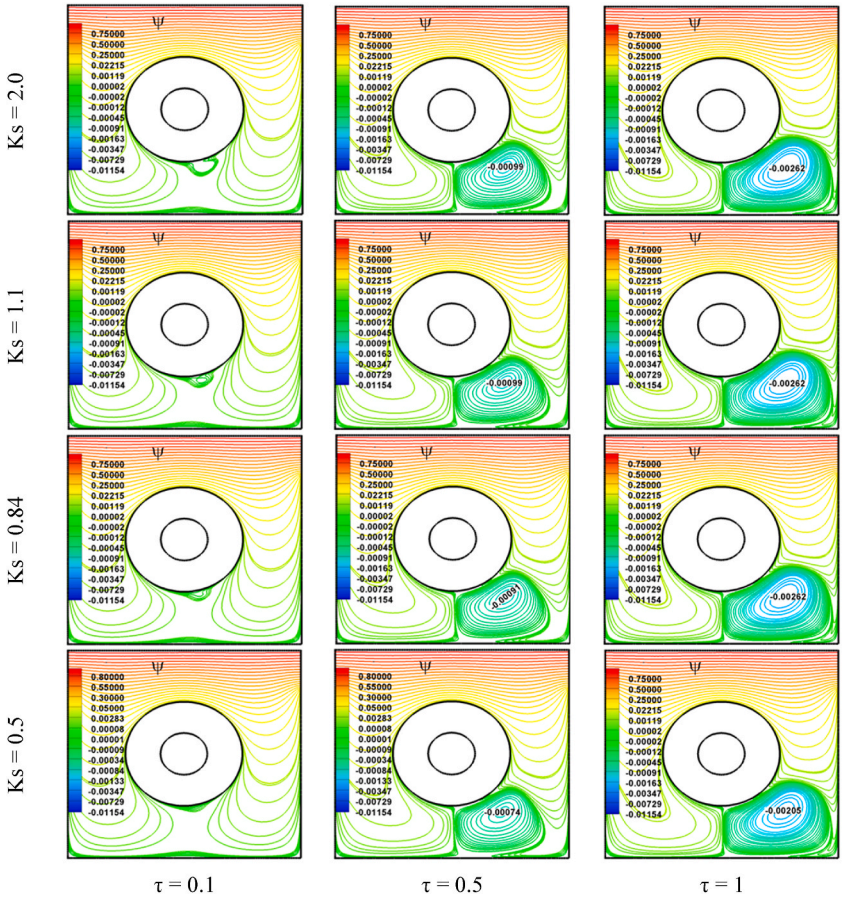

Fig. 4. Outcome of selected solid's thermal conductivity, (Ks = 0.5, 0.84, 1.1 and 2.0) and dimensionless time (τ = 0.1, 0.5, and 1) on streamlines at Ri = 1, Re = 100, D = 0.3, δ = 0.04 and φ = 2%.

with increasing value of τ as with time, the difference in temperature between a heated solid surface and a fluid reduces. However, after a certain value of τ, the system stability tends to be achieved with the rise in time, as seen by the flattening of the curve in Fig. 6. From Fig. 6(a), it can be detected that the value of Nu_{av} is maximum for a solid Ks = 0.5 thermal conductivity, which is owing to conjugate mixed-convection heat transfer is largely dependent on the inter-domain thermo-fluidic interaction due to the thermal conductivity of the inserted solid through the viscous behavior of the fluid chest, optimum fluid friction confirms better energy efficiency. Since fluid friction is observed to cross the critical limit in the current analysis, thermal exchange is increased along with the reduction of Ks. This situation is for the value range of τ = 0 to 0.5. As we approach dimensionless time τ = 1, Nu_{av} becomes almost the same for all values of Ks. The reason behind this is that as time passes by, most of the heat is conducted to the outside surface of the cylinder. The 3D plot in Fig. 6(b) gives a better understanding that the thermal exchange rate only becomes less and less with the increment of Ks. Also, it can be deduced that 27.3% heat transfer enhancement has been observed with the decreasing of Ks from 2 to 0.5 at τ = 0.5. From Fig. 6(b), it is 4clear by the 3D visualization that the surface heat transfer rate of the solid cylinder decreases as the thermal conductivity of the cylinder and dimensionless time increases. The conductive heat transfer that occurred coupled with the convective heat transfer through the solid cylinder to the working fluid is what caused it.

4.4. *Effect on shear rate*

Area-based integration for the determination of the Sh_{av} on the cylindrical surface is thought to be an important indicator of thermal performance evaluation. Shear rate is the pace at which the intended computational domain experiences incremental shearing deformation in thermodynamics. Fig. 7 presents the consequence of selected solid's thermal conductivity (Ks), and dimensionless component of time (τ) on the cylinder surface average shear rate (Sr). It can be spotted from Fig. 7(a) that when the value of Ks increases in a certain dimensionless time, the Sr value also increases. The basic reason behind this is that if the value of Ks is increased, the ability of heat conduction-the only way for heat to travel from the inner surface to the outer surface of the cylinder-is increased. So, heat is conducted to the outer surface from where fluid can take the heat away from it. This phenomenon increases the linear fluid velocity of the computational domain. Thus, the average shear rate is increased. Fig. 7(a) shows that with the increment of dimensionless time, the average shear rate on the cylindrical surface also increases. For τ = 0.5, increasing Ks from 0.5 to 2 reduces thermo-

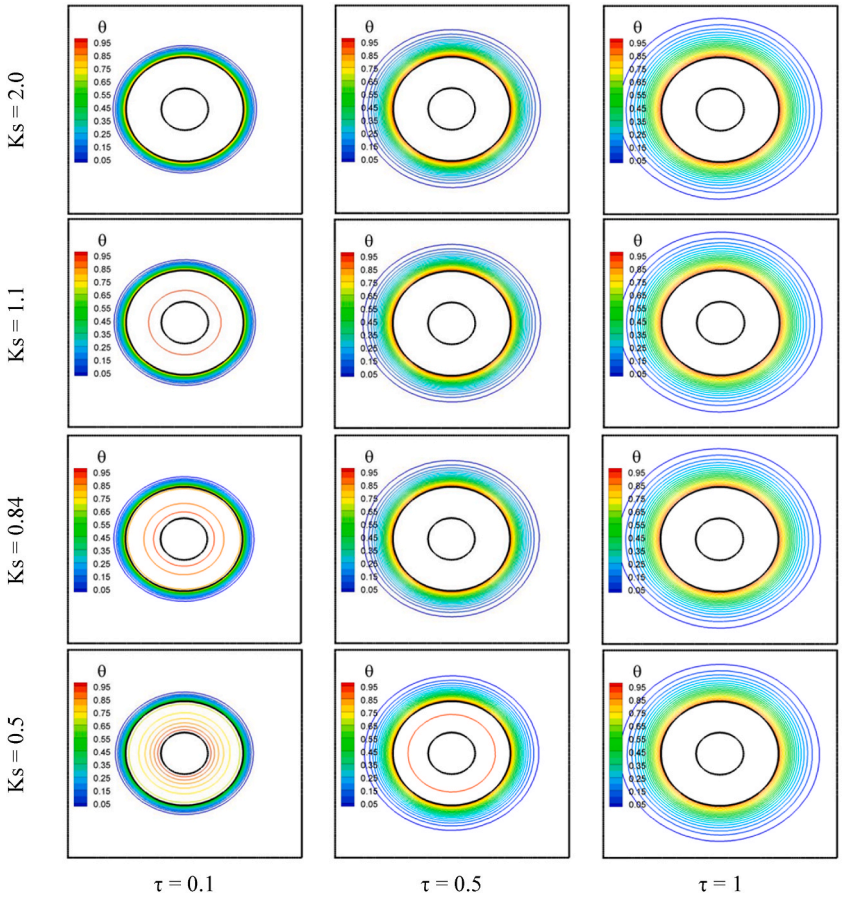

Fig. 5. Consequence of selected solid's thermal conductivity, (Ks = 0.5, 0.84, 1.1 and 2.0) and dimensionless time (τ = 0.1, 0.5, and 1) on isotherms at Ri = 1, Re = 100, D = 0.3, δ = 0.04 and φ = 2%.

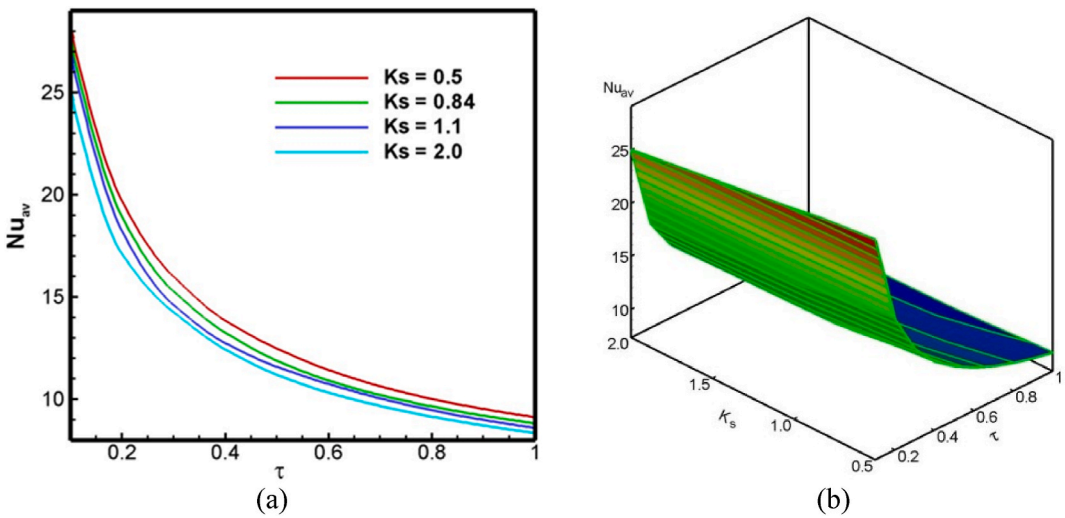

Fig. 6. Outcome of selected solid's thermal conductivity, Ks and dimensionless time τ on average Nusselt number from the heated surface of the heat source (a) line diagram and (b) Surface diagram.

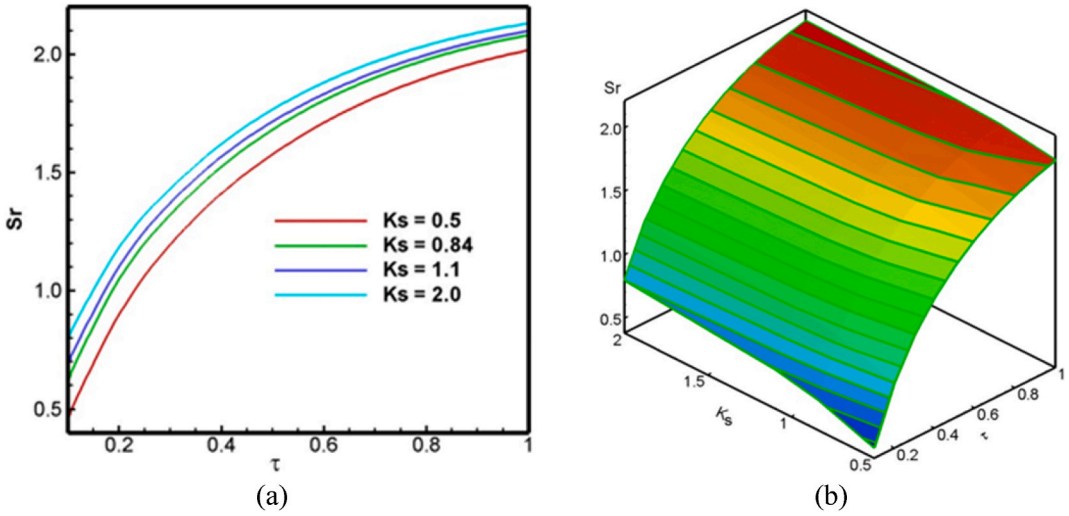

Fig. 7. Consequence of selected solid's Ks and τ on Sh_{av} on the cylinder surface (a) line diagram and (b) Surface diagram.

fluid performance through the increase of the value of Sr by 12.25%. Fig. 7(b) represents 3D modeling for Ks and τ on Sr which further aligns with the findings of Fig. 7(a). While inspecting Fig. 7(b), an evolution of the shear rate is observed with the simultaneous increase of τ and Ks which is ensuring the validity of the findings from Fig. 7(a).

4.5. Effect on bulk fluid temperature

Analysis of bulk fluid temperature is applied for evaluating thermo-fluid interactions in a unique manner as it is defined as a ratio of temperature to domain fluid density. The influence of thermal conductivity, Ks, of the solid material and dimensionless component of time on the fluid bulk temperature (θ_b) is presented in Fig. 8. The value of θ_b increases as the value of thermal conductivity of the solid increases in a specific dimensionless period, as shown in Fig. 8(a). The main reasoning behind this particular incident is that as the value of Ks rises, so does the ability of heat conduction, which is the only method for heat to pass from the cylinder's inner to exterior surfaces. As a result of this action, heat is transferred to the outer surface, where it may be removed by fluid. The equation for measuring θ_b also gives another reason for this finding. As the increment of the temperature inside the fluid domain decreases the density of the fluid, the bulk fluid temperature will be more if the fluid is more heated. Another thing to notice in Fig. 8(a) is that the fluid bulk temperature rises as the dimensionless time grows. Increasing Ks from 0.5 to 2 raises the fluid's bulk temperature by 16.3% for $\tau = 0.5$. The 3D modeling is shown in Fig. 8(b) which coincides with the findings in Fig. 8(a), proving the viability of the results.

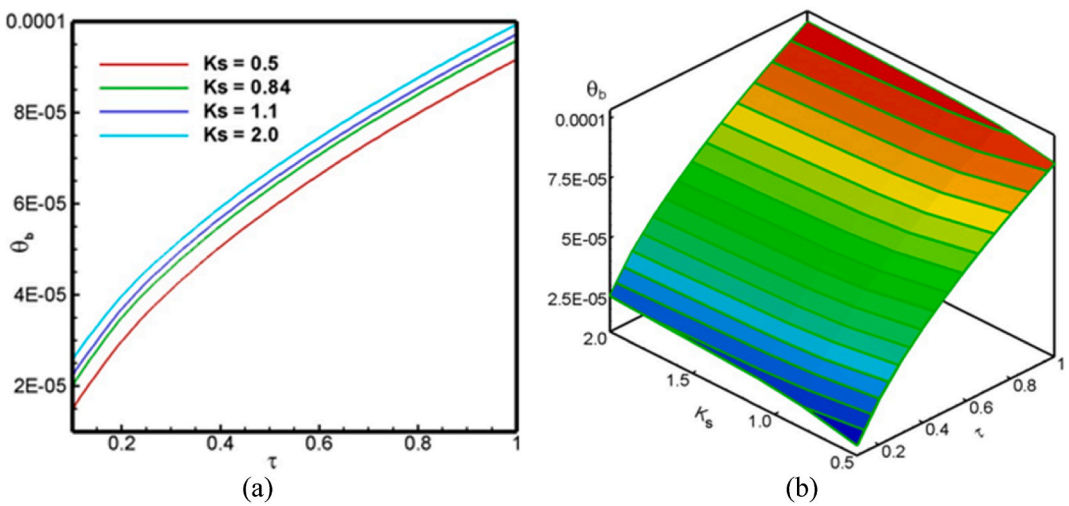

Fig. 8. Outcome of selected solid's Ks and τ on fluid bulk (a) line diagram and (b) Surface diagram.

4.6. Outcome on the pressure gradient

Fig. 9 illustrates the influences of solid's thermal conductivity (Ks), and τ on the fluid pressure gradient. From Fig. 9(a), it is ascertained that the value of the pressure gradient of the fluid domain is increasing with the increment value of Ks for a certain value of τ. As the fluid inside the cavity is being thermally induced by the heated outer surface of the annular cylinder, depends on how fast the fluid is being induced by the outside surface of the cylinder. If the value of Ks is increased, it becomes easier for the heat to be conducted from the inner to the outer surface of the cylinder. Another observation that can be made from this plot is that for a certain value of Ks, the value of the pressure gradient is increasing with dimensionless time. The forced nature of the flow is turning into mixed convection as the fluid is thermally induced by the heated cylinder and the flow is becoming more buoyancy induced. This decreases the flow strength, and the pressure gradient is thus increased with time. Increasing the value of Ks from 0.5 to 2 gives a 15.7% increment in the value of ∇P. In addition, the data obtained from the 3D model of Fig. 9(b) are observed to provide support to the above-mentioned findings from a holistic point of view.

4.7. Consequense on the velocity magnitude

In the mixed convection analysis, root means square (RMS) velocity magnitude explored to play a crucial role in determining the flow transformation. Moreover, not only the horizontal but also the vertical components of the velocity magnitude are defined to be passive scalars as they are significantly influenced by the thermal parameters. Fig. 10 shows the response of Ks and τ on the fluid domain's RMS velocity magnitude. From Fig. 10(a), it is detected that velocity magnitude is increasing with the increasing value of dimensionless time τ for a certain thermal conductivity. Because the fluid's velocity increases as its density increases over time. In addition, with the thermal conductivity, the RMS velocity increases. As the value of Ks increases the fluid temperature which is directly disproportional to the fluid density. Consequently, the fluid viscosity decreases which increases the fluid RMS velocity. The 3D plot in Fig. 10(b) reveals that for dimensionless time $\tau = 1$, there is a nearly 9.9% increase in the magnitude of the RMS velocity of the domain of fluid for the increment of Ks from 0.5 to 2.

4.8. Effect on the solid and fluid temperature gradient

The influence of Ks and τ on the temperature gradient of the fluid domain is shown in Fig. 11. Upon inspecting Fig. 11(a), it is evident that with the increment of τ, the temperature gradient for the fluid domain is increased. As the flow is introduced in the enclosure, it was forced by nature. Being thermally induced by the hot cylinder increases the temperature of the fluid. At time $\tau = 1$, the fluid is fully heated before leaving the enclosure with the help of the outlet. That is why the temperature gradient is increased with τ. Other things are to be noted that the value of temperature gradient also increased with the increment of Ks for a certain value of τ and a higher value of Ks (for instance Ks = 2), the change in temperature gradient is much less dynamic than for the lower value of Ks like Ks = 0.5 where heat transfer has been facilitated with the enhanced positive change of domain temperature gradient. According to the 3D figure in Fig. 11(b), an increase in thermal conductivity from 0.5 to 2 leads to a temperature gradient value difference of 24.5% for = 0.1. But for dimensionless time $\tau = 1$, this change is reduced to only 4.2%. This proves the previous point of temperature gradient value being much less dynamic for a higher value of Ks. The aftermath of Ks of 4 different solids on the temperature gradient in solid for different cases of dimensionless time (τ) is explored in Fig. 12. As can be seen from the plot of Fig. 12(a) that for $\tau = 0.1$, the highest temperature gradient can be seen from a solid that has the lowest thermal conductivity (Ks). The reason behind this is because of low thermal conductivity, the temperature difference concerning the length between the inner and the outer surface of the cylinder is

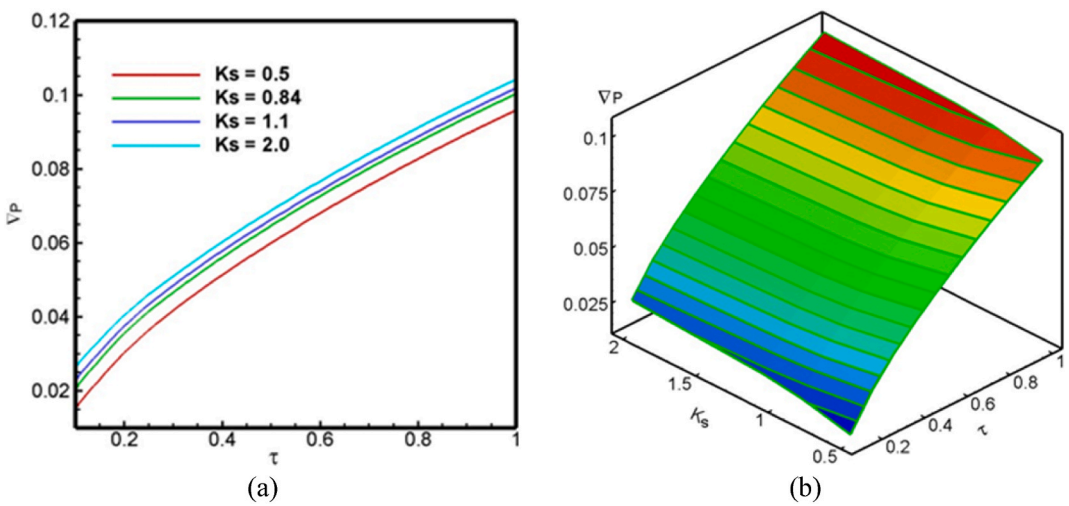

Fig. 9. Consequence of selected solid's Ks and τ on fluid pressure (a) line diagram and (b) Surface diagram.

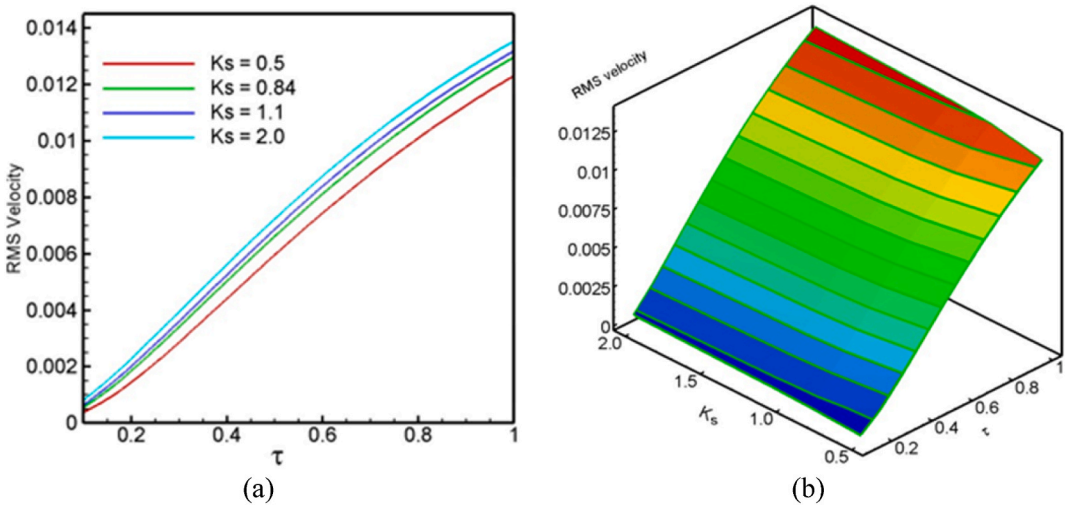

Fig. 10. Outcome of selected solid's Ks and τ on RMS velocity in fluid domain (a) line diagram and (b) Surface diagram.

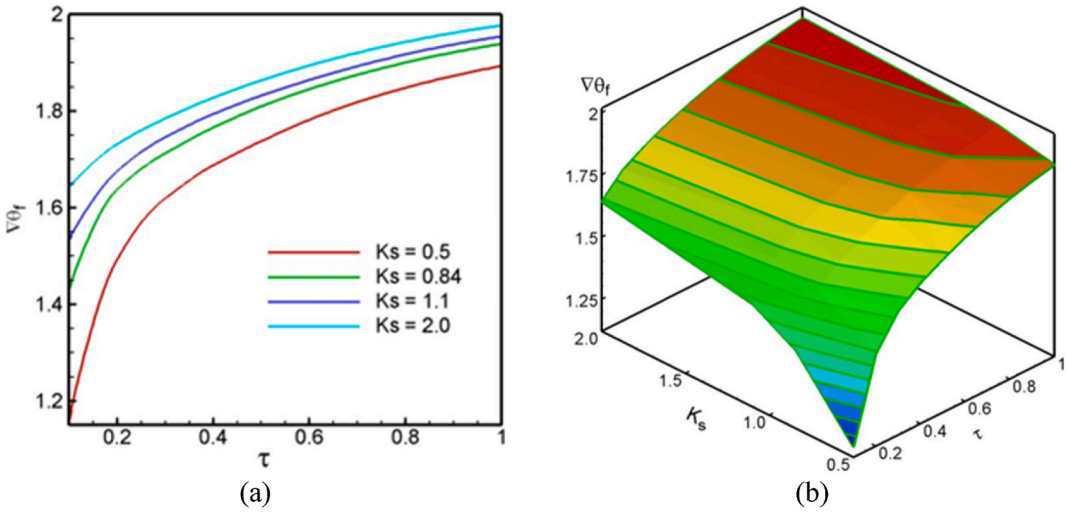

Fig. 11. Consequence of selected solid's thermal conductivity, Ks and dimensionless time, τ on fluid domain temperature gradient (a) line diagram and (b) Surface diagram.

greater. If the solid has much higher thermal conductivity (for instance, Ks = 2), the temperature difference is readily mended as heat conductance is much higher for this case. If the plot is observed for a certain Ks, it is clear that with an increment of dimensionless time, the temperature gradient in the solid is getting lowered. In fact, the temperature gradient is almost 0 and this is true for almost all four solids. As time passes by, the whole cylinder is uniformly heated which doesn't give much scope for temperature difference across the periphery of the cylinder. Fig. 12(b) shows the 3D plot from where it is noticed that for dimensionless time τ = 0.1, there is almost a multiplier of 53.4 increase in the temperature gradient in solid for the increment of Ks from 0.5 to 2. This gives clear insurance that the solid's thermal conductivity has a dominant effect on not only the fluid domain but also the solid domain temperature gradient.

4.9. Effect on exit fluid temperature

Fig. 13 shows the significance of four selected solid's Ks and τ on the average fluid exit fluid temperature of the enclosure inside the fluid domain. From Fig. 13(a) it is observed that no change in fluid exit temperature when the time τ is fluctuated between 0 and 0.5. But going forward there is a significant change in the exit temperature. The main reason behind this is that conduction of heat from the inner to the outer circle of the cylinder takes time which is why there is no change in exit fluid temperature at the beginning. But when the outer surface is heated, the corresponding convective domain is also heated, and thus the exit fluid temperature increases. For dimensionless time τ = 1, there is almost a 42.8% increase in θ_{exit} for the increment of Ks from 0.5 to 2. Moreover, a 33.3% decrease in exit fluid temperature has been recorded with the decrease of Ks from 2 to 0.5 as lowering Ks is supposed to facilitate thermal

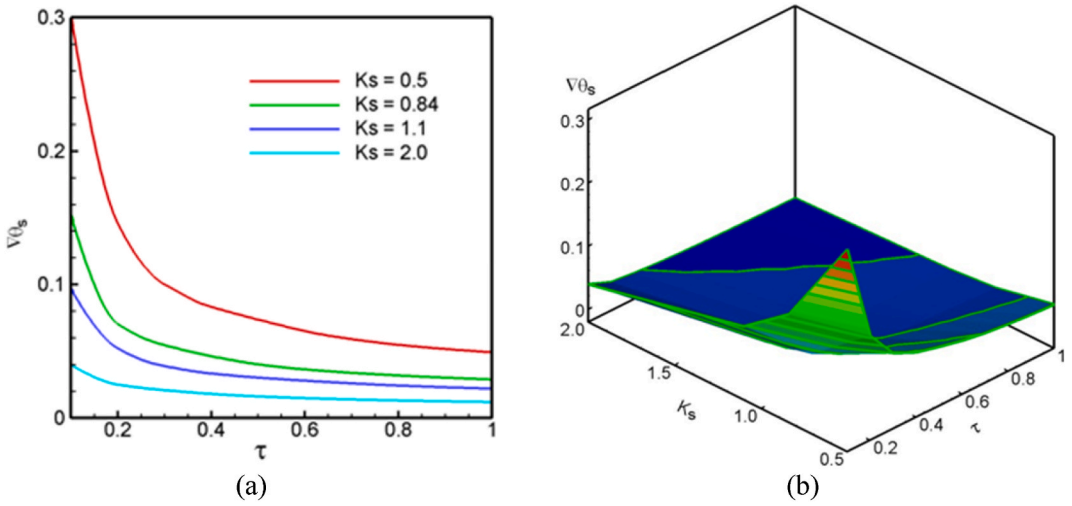

Fig. 12. Outcome of selected solid's thermal conductivity, Ks and dimensionless time, τ on solid domain temperature gradient (a) line diagram and (b) Surface diagram.

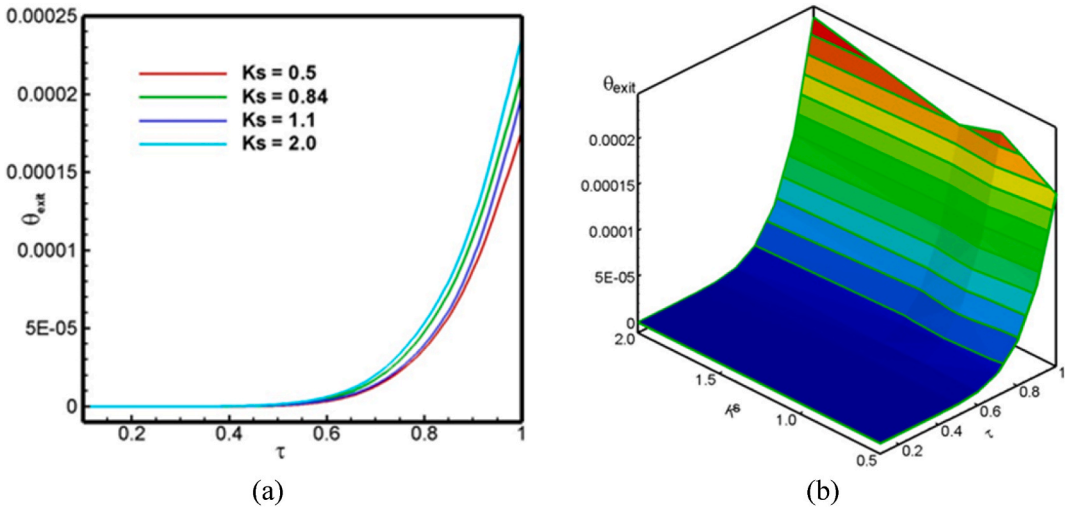

Fig. 13. Consequence of selected solid's thermal conductivity, Ks and dimensionless time, τ on the average exit port fluid temperature of the enclosure (a) line diagram and (b) Surface diagram.

performance through the maintenance of optimum friction in the fluid chest. The 3D plot in Fig. 13(b) gives a better understanding that the exit fluid temperature only becomes more and more with the increment of Ks. Upon inspecting the 3D plot in Fig. 13(b), it is more incisive to point out that the exit fluid temperature increases for the inner surface of the cylinder as the Ks and τ increases.

4.10. Effect on vortices

A pseudo-vector field that characterizes the local rotating motion of a continuum around a point as viewed by an observer moving with the flow is known as the vorticity. Fig. 14 presents the outcome of the cylinder thermal conductivity (Ks) on the vorticity in fluid for a range of values of dimensionless time (τ). From Fig. 14(a), it is evident that the vorticity value decreases over dimensionless time for all *Ks* of solid and the lowest value of *Ks* of solid has the highest value of vortices. As per the equation, the value of vorticity is calculated by subtraction of the different co-ordinate-based differential components of the horizontal stream function component from the vertical component. In the current mixed convection system with an inlet and outlet, flow is tending to be one-directional due to the transient to the steady transformation of the system. Moreover, the horizontal component of the stream function is getting bigger with the increment of time as the flow is being thermally induced from the cylinder. That is why the value of vortices is getting lowered. Also, by lowering the thermal conductivity, the flow of fluid inside the enclosure has the chance of getting properly heated which also increases the vertical stream function component. So, the lowest value of solid's thermal conductivity gives the highest values of

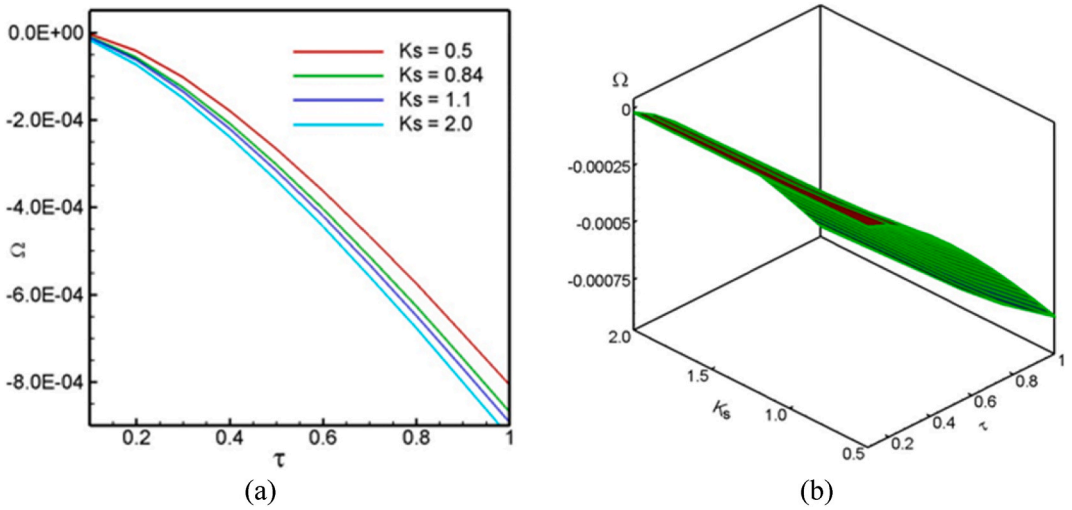

Fig. 14. Outcome of selected solid's Ks and τ on the value of vorticity inside the enclosure (a) line diagram and (b) Surface diagram.

vortices. For dimensionless time $\tau = 1$, decreasing the value of Ks from 2 to 0.5 gives a 12.5% increment in the value of the vortices of the fluid domain which is obtained from the 3D plot of Fig. 14(b) where the subsequent graphs are observed having a good compliance with the quantitative results found in Fig. 14(a).

4.11. Heat transfer correlation

The mean Nusselt numbers described in Fig. 6 are mathematically related to thermal conductivity Ks and time τ. In the correlation, Average heat transfer rate is presented in terms of the independent variables Ks and τ. The range of the input variables are $0.5 \leq Ks \leq 2$ and $0.1 \leq \tau \leq 1$. The derived correlation is presented below:

$$Nu_{av} = 0.4753Ks + 1.8845\tau + 5.0285 \tag{32}$$

From equation it is observed that average heat transfer rate is proportionally related with conductivity of the solid and time τ.

5. Conclusion

In this particular study, the significance of thermal conductivity and transient analysis of four low conductive materials for the annular design on mixed convection in a vented cavity are investigated. Plastic tiles (Ks = 0.5), Clay tiles (Ks = 0.84), Concrete tiles (Ks = 1.1) and Slate tiles (Ks = 2) are applied as cylinder materials with a variation of time, τ from 0 to 1. Thermal and hydrodynamic properties are analyzed for 2% CNT-water nanofluid at Ri = 1, Re = 100, D = 0.3 and δ = 0.04. Moreover, surface and 3D plots are also included for ensuring the reliability of the findings in a holistic sense. The following concluding remarks are provided to summarize the findings of this study:

- ●Heat transfer from the heated surface of the cylinder is enhanced by 27.3% with a decrease of Ks from 2 to 0.5 at τ = 0.5.
- ●With an increase of Ks, a 12.25% increase in shear rate is noticed at τ = 0.5 for the cylindrical surface.
- ●At τ = 0.1, a 24.5% increment of the fluid temperature gradient is observed varying Ks from 0.5 to 2 where the final difference is reduced to 4.2% at τ = 1. However, for a similar variation of Ks, 53.4% increment of the solid temperature gradient is traced at τ = 0.1.
- ●Increasing the value of Ks results in a 15.7% and 9.9% increase in fluid pressure gradient and velocity magnitude respectively. On the other hand, vortex strength has been enhanced by 12.5% through the decrease of Ks value from 2 to 0.5 at τ = 1.
- ●Overall, 42.8% enhancement of the exit fluid temperatures has been noticed with the increase of Ks.
- ●Increasing Ks from 0.5 to 2 raises the fluid's bulk temperature by 16.3% for τ = 0.5.
- ●Qualitative isotherm and streamline contours are significantly influenced by thermal conductivity. While a 33% increase in flow field strength is recorded for raising Ks 0.5 to1.1. The fluid temperature along the heated wall, on the other hand, has practically quadrupled.

Author contribution statement

M.M. Rahman: Conceived and designed the experiments; Performed the experiments; Analyzed and interpreted the data; Contributed reagents, materials, analysis tools or data.

Mohedul Hasan; A.K. Azad: Conceived and designed the experiments; Performed the experiments; Wrote the paper.

Shadman Sakib Priam; Abrar Nur-E Faiaz: Analyzed and interpreted the data; Contributed reagents, materials, analysis tools or data; Wrote the paper.

Funding statement

This research did not receive any specific grant from funding agencies in the public, commercial, or not-for-profit sectors.

Data availability statement

No data was used for the research described in the article.

Declaration of interest's statement

The authors declare no conflict of interest.

Acknowledgment

The authors wish to express their appreciation to the CFD Research Group of the Department of Mathematics, the CFDHT Research Group of the Department of Mechanical Engineering in Bangladesh University of Engineering and Technology and Department of Natural Sciences of Islamic University of Technology for providing the incessant support.

References

[1] A. Kalam, J.H. Munshi, M. Rahman, M.M.K. Chowdhury, Analysis of combined convection in an open cavity under constant heat flux boundary conditions and magnetic field using finite element method, J. Sci. Res. 6 (2) (Apr. 2014) 243–256, https://doi.org/10.3329/JSR.V6I2.14505.

[2] S. Sivasankaran, V. Sivakumar, A.K. Hussein, P. Prakash, *10.1080/10407782.2013.826017*, Mixed Convection in a Lid-Driven Two-Dimensional Square Cavity with Corner Heating and Internal Heat Generation 65 (3) (2013) 269–286, https://doi.org/10.1080/10407782.2013.826017. Feb.

[3] A.K. Kareem, H.A. Mohammed, A.K. Hussein, S. Gao, Numerical investigation of mixed convection heat transfer of nanofluids in a lid-driven trapezoidal cavity, Int. Commun. Heat Mass Tran. 77 (Oct. 2016) 195–205, https://doi.org/10.1016/J.ICHEATMASSTRANSFER.2016.08.010.

[4] M. November, M.W. Nansteel, Natural convection in rectangular enclosures heated from below and cooled along one side, Int. J. Heat Mass Tran. 30 (11) (1987) 2433–2440, Nov, https://doi.org/10.1016/0017-9310(87)90233-X.

[5] A. Valencia, R.L. Frederick, Heat transfer in square cavities with partially active vertical walls, Int. J. Heat Mass Tran. 32 (8) (1989) 1567–1574, Aug, https://doi.org/10.1016/0017-9310(89)90078-1.

[6] J.M. House, C. Beckermann, T.E. Smith, Effect Of A Centered Conducting Body On Natural Convection Heat Transfer In An Enclosure, 2010, pp. 213–225, https://doi.org/10.1080/10407789008944791, vol. 18, no. 2.

[7] A.K. Hussein, H.K. Hamzah, F.H. Ali, L. Kolsi, Mixed convection in a trapezoidal enclosure filled with two layers of nanofluid and porous media with a rotating circular cylinder and a sinusoidal bottom wall, J. Therm. Anal. Calorim. 141 (5) (2020) 2061–2079, Sep, https://doi.org/10.1007/S10973-019-08963-6/FIGURES/13.

[8] H. Laouira, F. Mebarek-Oudina, A.K. Hussein, L. Kolsi, A. Merah, O. Younis, Heat transfer inside a horizontal channel with an open trapezoidal enclosure subjected to a heat source of different lengths, Heat Tran. Res. 49 (1) (Jan. 2020) 406–423, https://doi.org/10.1002/HTJ.21618.

[9] A.A.A.A. Al-Rashed, et al., Mixed convection and entropy generation in a nanofluid filled cubical open cavity with a central isothermal block, Int. J. Mech. Sci. 135 (Jan. 2018) 362–375, https://doi.org/10.1016/J.IJMECSCI.2017.11.033.

[10] S.E. Ahmed, M.A. Mansour, A.K. Hussein, B. Mallikarjuna, M.A. Almeshaal, L. Kolsi, MHD mixed convection in an inclined cavity containing adiabatic obstacle and filled with Cu–water nanofluid in the presence of the heat generation and partial slip, J. Therm. Anal. Calorim. 138 (2) (2019) 1443–1460, Oct, https://doi.org/10.1007/S10973-019-08340-3/FIGURES/19.

[11] T. Basak, S. Roy, A.R. Balakrishnan, Effects of thermal boundary conditions on natural convection flows within a square cavity, Int. J. Heat Mass Tran. 49 (23–24) (2006) 4525–4535, Nov, https://doi.org/10.1016/J.IJHEATMASSTRANSFER.2006.05.015.

[12] S. Izadi, T. Armaghani, R. Ghasemiasl, A.J. Chamkha, M. Molana, A comprehensive review on mixed convection of nanofluids in various shapes of enclosures, Powder Technol. 343 (Feb. 2019) 880–907, https://doi.org/10.1016/J.POWTEC.2018.11.006.

[13] W. Al-Kouz, et al., Effect of a rotating cylinder on the 3D MHD mixed convection in a phase change material filled cubic enclosure, Sustain. Energy Technol. Assessments 51 (2022), https://doi.org/10.1016/J.SETA.2021.101879, 101879, Jun.

[14] S.S. Priam, R. Nasrin, Oriented magneto-conjugate heat transfer and entropy generation in an inclined domain having wavy partition, Int. Commun. Heat Mass Tran. 126 (2021), https://doi.org/10.1016/J.ICHEATMASSTRANSFER.2021.105430, 105430, Jul.

[15] S.S. Priam, M.M. Ikram, S. Saha, S.C. Saha, Conjugate natural convection in a vertically divided square enclosure by a corrugated solid partition into air and water regions, Therm. Sci. Eng. Prog. 25 (2021), https://doi.org/10.1016/J.TSEP.2021.101036, 101036, Oct.

[16] L.S. Sundar, K.V. Sharma, M.K. Singh, A.C.M. Sousa, Hybrid nanofluids preparation, thermal properties, heat transfer and friction factor – a review, Renew. Sustain. Energy Rev. 68 (Feb. 2017) 185–198, https://doi.org/10.1016/J.RSER.2016.09.108.

[17] S.M. Saeidi, J.M. Khodadadi, Forced convection in a square cavity with inlet and outlet ports, Int. J. Heat Mass Tran. 49 (11–12) (2006) 1896–1906, Jun, https://doi.org/10.1016/J.IJHEATMASSTRANSFER.2005.10.033.

[18] B. Ali, S. Hussain, Y. Nie, A.K. Hussein, D. Habib, Finite element investigation of Dufour and Soret impacts on MHD rotating flow of Oldroyd-B nanofluid over a stretching sheet with double diffusion Cattaneo Christov heat flux model, Powder Technol. 377 (Jan. 2021) 439–452, https://doi.org/10.1016/J.POWTEC.2020.09.008.

[19] F. Selimefendigil, H.F. Öztop, Forced convection of ferrofluids in a vented cavity with a rotating cylinder, Int. J. Therm. Sci. 86 (Dec. 2014) 258–275, https://doi.org/10.1016/J.IJTHERMALSCI.2014.07.007.

[20] R. Iwatsu, J.M. Hyun, K. Kuwahara, Mixed convection in a driven cavity with a stable vertical temperature gradient, Int. J. Heat Mass Tran. 36 (6) (1993) 1601–1608, https://doi.org/10.1016/S0017-9310(05)80069-9.

[21] S. Singh, M.A.R. Sharif, Mixed Convective Cooling Of A Rectangular Cavity With Inlet And Exit Openings On Differentially Heated Side Walls, 2011, pp. 233–253, https://doi.org/10.1080/716100509, vol. 44, no. 3.

[22] D. Chatterjee, B. Mondal, P. Halder, Hydromagnetic Mixed Convective Transport in a Vertical Lid-Driven Cavity Including a Heat Conducting Rotating Circular Cylinder, 2013, pp. 48–65, https://doi.org/10.1080/10407782.2013.812399, vol. 65, no. 1.

[23] V.M. Job, S.R. Gunakala, A.J. Chamkha, Numerical investigation of unsteady MHD mixed convective flow of hybrid nanofluid in a corrugated trapezoidal cavity with internal rotating heat-generating solid cylinder, Eur. Phys. J. Spec. Top. (2022) 1–8, https://doi.org/10.1140/EPJS/S11734-022-00604-8. May 2022.
[24] M.M. Rahman, M.A. Alim, M.A.H. Mamun, Finite element analysis of mixed convection in a rectangular cavity with a heat-conducting horizontal circular cylinder, Nonlinear Anal. Model Control 14 (2) (2009) 217–247.
[25] M. Lacroix, A. Joyeux, Natural convection heat transfer around two heated cylinders in an isothermal enclosure including the effect of wall conductance, Int. J. Numer. Methods Heat Fluid Flow 4 (5) (May 1994) 465–476, https://doi.org/10.1108/EUM0000000004050/FULL/XML.
[26] M. Lacroix, A. Joyeux, Natural Convection Heat Transfer Around Heated Cylinders Inside A Cavity With Conducting Walls, 2007, pp. 335–349, https://doi.org/10.1080/10407789508913704, vol. 27, no. 3.
[27] C. Butler, D. Newport, M. Geron, Natural convection experiments on a heated horizontal cylinder in a differentially heated square cavity, Exp. Therm. Fluid Sci. 44 (Jan. 2013) 199–208, https://doi.org/10.1016/J.EXPTHERMFLUSCI.2012.06.009.
[28] P. Estellé, O. Mahian, T. Maré, H.F. Öztop, Natural convection of CNT water-based nanofluids in a differentially heated square cavity, J. Therm. Anal. Calorim. 128 (3) (2017) 1765–1770, Jun, https://doi.org/10.1007/S10973-017-6102-1/FIGURES/4.
[29] A.A.A.A. Al-Rashed, et al., Three-dimensional investigation of the effects of external magnetic field inclination on laminar natural convection heat transfer in CNT–water nanofluid filled cavity, J. Mol. Liq. 252 (Feb. 2018) 454–468, https://doi.org/10.1016/J.MOLLIQ.2018.01.006.
[30] M. Hamid, Z.H. Khan, W.A. Khan, R.U. Haq, Natural convection of water-based carbon nanotubes in a partially heated rectangular fin-shaped cavity with an inner cylindrical obstacle, Phys. Fluids 31 (10) (2019), https://doi.org/10.1063/1.5124516, 103607, Oct.
[31] F. Selimefendigil, H.F. Öztop, Corrugated conductive partition effects on MHD free convection of CNT-water nanofluid in a cavity, Int. J. Heat Mass Tran. 129 (Feb. 2019) 265–277, https://doi.org/10.1016/j.ijheatmasstransfer.2018.09.101.
[32] S.K. Gupta, D. Chatterjee, B. Monda, Investigation of Mixed Convection in a Ventilated Cavity in the Presence of a Heat Conducting Circular Cylinder, 2014, pp. 52–74, https://doi.org/10.1080/10407782.2014.916113, vol. 67, no. 2.
[33] S.S. Priam, R. Saha, S. Saha, Pure mixed convection inside a vented square cavity with an isothermally heated rotating cylinder, AIP Conf. Proc. 2324 (1) (2021), https://doi.org/10.1063/5.0037533, 050035, Feb.
[34] A.N.E. Faiaz, S.S. Priam, A. Shahriar, M.A.H. Mamun, Conjugate mixed convective flow of Gallium in a partially vented square cavity in the presence of a rotating cylinder, ASME Int. Mech. Eng. Congr. Expo. Proc. 11 (Jan) (2022), https://doi.org/10.1115/IMECE2021-73254.
[35] M.A.H. Mamun, M.M. Rahman, M.M. Billah, R. Saidur, A numerical study on the effect of a heated hollow cylinder on mixed convection in a ventilated cavity, Int. Commun. Heat Mass Tran. 37 (9) (2010) 1326–1334, Nov, https://doi.org/10.1016/J.ICHEATMASSTRANSFER.2010.07.019.
[36] T. Tayebi, A.J. Chamkha, Entropy generation analysis due to MHD natural convection flow in a cavity occupied with hybrid nanofluid and equipped with a conducting hollow cylinder, J. Therm. Anal. Calorim. 139 (3) (2020) 2165–2179, Feb, https://doi.org/10.1007/S10973-019-08651-5/FIGURES/12.
[37] M.F. Karim, S. Huq, A.K. Azad, M.S.R. Chowdhury, M.M. Rahman, Numerical analysis of thermofluids inside a porous enclosure with partially heated wall, Int. J. Thermofluids 11 (2021), https://doi.org/10.1016/J.IJFT.2021.100099, 100099, Aug.
[38] S.T. Keya, S. Yeasmin, M.M. Rahman, M.F. Karim, M.R. Amin, Mixed convection heat transfer in a lid-driven enclosure with a double-pipe heat exchanger, Int. J. Thermofluids 13 (2022), https://doi.org/10.1016/J.IJFT.2021.100131, 100131, Feb.
[39] M.A. Ismael, H.F. Jasim, Role of the fluid-structure interaction in mixed convection in a vented cavity, Int. J. Mech. Sci. 135 (Jan. 2018) 190–202, https://doi.org/10.1016/J.IJMECSCI.2017.11.001.
[40] A.K. Azad, M.M. Shuvo, R.H. Kabir, K.M. Rabbi, M.F. Karim, M.M. Rahman, Heat transfer augmentation in a diamond shaped enclosure utilizing CNT-water Nanofluid, Int. Commun. Heat Mass Tran. 116 (2020), https://doi.org/10.1016/J.ICHEATMASSTRANSFER.2020.104647, 104647, Jul.
[41] R. Hossain, A.K. Azad, M. Jahid Hasan, M.M. Rahman, Thermophysical properties of Kerosene oil-based CNT nanofluid on unsteady mixed convection with MHD and radiative heat flux, Eng. Sci. Technol. an Int. J. 35 (2022), https://doi.org/10.1016/J.JESTCH.2022.101095, 101095, Nov.
[42] K.S. Al Kalbani, M.S. Alam, M.M. Rahman, Finite element analysis of unsteady natural convective heat transfer and fluid flow of nanofluids inside a tilted square enclosure in the presence of oriented magnetic field, Am. J. Heat Mass Transf. 3 (3) (2016) 186–224, https://doi.org/10.7726/ajhmt.2016.1012.
[43] R. Hossain, A.K. Azad, M.J. Hasan, M.M. Rahman, Radiation effect on unsteady MHD mixed convection of kerosene oil-based CNT nanofluid using finite element analysis, *Alexandria Eng. J.*, Feb. (2022), https://doi.org/10.1016/J.AEJ.2022.02.005.
[44] I. Tosun, Evaluation of transfer coefficients: engineering correlations, Model. Transp. Phenom. (Jan. 2007) 59–115, https://doi.org/10.1016/B978-044453021-9/50005-1.
[45] A. Azad, MHD Combined Convection in a Channel with Cavity Using Nanofluids, 2016.
[46] A.J. Chamkha, S.H. Hussain, Q.R. Abd-Amer, Mixed Convection Heat Transfer of Air inside a Square Vented Cavity with a Heated Horizontal Square Cylinder, 2011, pp. 58–79, https://doi.org/10.1080/10407782.2011.541216, vol. 59, no. 1.
[47] K.M. Shirvan, M. Mamourian, R. Ellahi, Numerical investigation and optimization of mixed convection in ventilated square cavity filled with nanofluid of different inlet and outlet port, Int. J. Numer. Methods Heat Fluid Flow 27 (9) (2017) 2053–2069, https://doi.org/10.1108/HFF-08-2016-0317/FULL/PDF.